Rapid Normal Stress Oscillations Cause Weakening and Anelastic Dilation in Gouge-Bearing Faults

Chen, Jianye; Niemeijer, Andre R.; Spiers, Christopher J.

DOI
10.1029/2024GL109755

Publication date
2024

Document Version
Final published version

Published in
Geophysical Research Letters

AGU ADVANCING EARTH AND SPACE SCIENCES

Geophysical Research Letters

RESEARCH LETTER
10.1029/2024GL109755

Key Points:
- We observed dynamic weakening and dilation of shearing gouges subjected to rapid oscillations in normal stress
- Fault compaction/dilation explains the shear stress evolution in response to different modes of normal stress perturbation
- We propose a micromechanical model for gouge friction under time-variable normal stress conditions

Supporting Information:
Supporting Information may be found in the online version of this article.

Correspondence to:
J. Chen,
j.chen3@uu.nl

Citation:
Chen, J., Niemeijer, A. R., & Spiers, C. J. (2024). Rapid normal stress oscillations cause weakening and anelastic dilation in gouge-bearing faults. *Geophysical Research Letters*, *51*, e2024GL109755. https://doi.org/10.1029/2024GL109755

Received 2 MAY 2024
Accepted 11 JUN 2024

Rapid Normal Stress Oscillations Cause Weakening and Anelastic Dilation in Gouge-Bearing Faults

Jianye Chen[1,2,3], Andre R. Niemeijer[2], and Christopher J. Spiers[2]

[1]State Key Laboratory of Earthquake Dynamics, Institute of Geology, China Earthquake Administration, Beijing, China, [2]HPT Laboratory, Department of Earth Sciences, Utrecht University, Utrecht, The Netherlands, [3]Faculty of Civil Engineering and Geosciences, Technical University of Delft, Delft, The Netherlands

Abstract Fault normal stress (σ_n) changes dynamically during earthquakes. However, the impact of these changes on fault strength is poorly understood. We explore the effects of rapidly varying σ_n by conducting rotary-shear experiments on simulated fault gouges at 1 μm/s, under well-drained, hydrothermal conditions. Our results show both elastic and anelastic (time-dependent but recoverable) changes in gouge layer thickness in response to step changes and sinusoidal oscillations in σ_n. In particular, we observe dilation associated with marked weakening during ongoing σ_n-oscillations at frequencies >0.1 Hz. Moreover, recovery of shear stress after such oscillations is accompanied by transient (anelastic) compaction. We propose a microphysically based friction model that explains most of the observations made, including the effects of temperature and step versus sinusoidal perturbation modes. Our results highlight that σ_n-oscillations above a specific frequency threshold, controlled by the loading regime and frictional properties of the fault, may enhance seismic hazards.

Plain Language Summary Faults in the crust sometimes experience rapid stress changes, caused by nearby or remote earthquakes, by seasonal impoundment and discharge of reservoirs, by hydrocarbon or geothermal energy production, or by reservoir stimulation. The impact of these stress changes on the earthquake potential of faults is poorly understood. This study explores such effects through laboratory experiments on simulated faults under upper crustal PT conditions, perturbing the normal stress on the fault in various ways. Our results show that the shear stress supported by the fault, and the fault thickness, respond instantly to normal stress changes, followed by a transient evolution. In particular, we observed dilation (fault-normal expansion) associated with marked weakening during fast oscillation. We propose a micromechanical model that can qualitatively explain the general experimental observations. Our results indicate that varying the normal stress on a fault at frequencies above a specific threshold may enhance seismic hazard.

1. Introduction

Tectonic fault zones are subject to variations in effective normal stress (σ_n^e) over a wide range of spatial and temporal scales. For example, stress can transfer between faults in the same system through elastic or viscoelastic coupling. Remote large earthquakes, emitting elastic waves that propagate thousands of kilometers, can dynamically trigger fault instability (Hill et al., 1993). Fluid pressures within a fault zone are expected to vary spatially and temporally during the seismic cycle, due to compaction, cementation, and fluid-rock interactions, which coupled with pressure diffusion and dilatant shearing can promote or delay fault failure (Noël et al., 2019; Segall & Rice, 1995; Sleep, 1997). External forcing by solid tides or seasonal impoundment and discharge of reservoirs can also modify the temporal evolution and spatial pattern of fault zone stresses. Moreover, human activities such as hydrocarbon and geothermal energy production, and injection of pressurized fluids such as CO_2 or (waste)water into deep reservoir systems, can change the stress field around faults, through both fluid pressure diffusion and poroelasticity, -potentially inducing earthquakes (e.g., Ellsworth, 2013). Resolving these scenarios requires a better understanding of the frictional stability of a fault in response to perturbations in stress, in particular in effective normal stress (defined as $\sigma_n^e = \sigma_n - p_f$, where σ_n and p_f are the normal stress and fluid pressure acting on and within the fault, respectively.)

Laboratory and numerical experiments offer potential ways to move forward. Early experimental studies of how fault strength and stability respond to σ_n^e-perturbations were performed on bare, nominally-dry rock surfaces (Bureau et al., 2000; Cochard et al., 2003; Linker & Dieterich, 1992; Olsson, 1988; Prakash, 1998). All of these experiments involved step or frequent sinusoidal changes (<1 s in period) in external normal load (σ_n) imposed on an already slipping fault. They showed that the frictional response to a rapid change in σ_n is a multistage (elastic/transient) process. Based on such work, Linker and Dieterich (1992) extended the classical rate-and-state friction (RSF) laws to describe the evolution of friction in response to σ_n-changes. Later studies have explored a variety of experimental materials (bare-rock surfaces, gouges) and perturbation modes (steps, pulses, and oscillations) (Boettcher & Marone, 2004; Dang & Konietzky, 2022; Griffa et al., 2013; Hong & Marone, 2005; Johnson et al., 2012; Kilgore et al., 2012, 2017; Lockner & Beeler, 1999; Shreedharan et al., 2019). More recently, an increasing number of experimental studies focus on the effects of varying fluid pressure (p_f) on fault stability (Cappa et al., 2019; French et al., 2016; Noël et al., 2019; Passelègue et al., 2018; Scuderi & Collettini, 2016; Scuderi et al., 2017), as an analogue for activation of fault slip by fluid injection into reservoirs or geothermal systems. The results showed that slip acceleration on a fault is controlled by the effective normal stress on the fault and sometimes by fluid injection rate (e.g., French et al., 2016; Wang et al., 2020). A more general finding is that time-varying σ_n or p_f can cause a transient response in friction, though promotion of unstable slip is not generally observed (Beeler & Lockner, 2003; Boettcher & Marone, 2004; Chambon & Rudnicki, 2001), except in some studies of bare surfaces (Noël et al., 2019). This is likely because all previous experiments were performed at room temperature, where most rock-forming minerals exhibit velocity (v) strengthening friction (Johnson et al., 2012; Xing et al., 2019), although other factors, such as apparatus stiffness, may also play a role (Boettcher & Marone, 2004). In velocity-strengthening materials, faults are frictionally stable, since any perturbation favoring slip acceleration is suppressed, even if the fault is critically-stressed. Progress into the unstable slip regime has been impeded by the technical challenge of achieving fast σ_n^e-variations under crustal temperature conditions where frictional fault slip is velocity weakening.

To provide the crucial data needed, we performed gouge-shearing experiments, at room and at in-situ crustal temperatures, to determine how σ_n^e-variations affect the frictional response of a fluid-saturated, gouge-filled carbonate fault under velocity-weakening conditions. The results demonstrate that rapidly varying normal stress causes a marked shear strength reduction, associated with a tendency for fault dilation, which may be key for understanding earthquake triggering.

2. Material and Method

2.1. Material and Experimental Apparatus

We conducted friction experiments on two types of simulated calcite-dolomite fault gouge using a hydrothermal, rotary-shear apparatus (Niemeijer et al., 2008). The materials used are described by Chen et al. (2015) and Verberne et al. (2013). The piston-sample assembly is fluid-pressure-compensated within the hydrothermal pressure vessel, so that the (Terzaghi) effective normal stress σ_n^e, acting on the sample layer, is obtained directly from the externally applied normal load. The hydrothermal machine is housed inside a commercial Instron loading frame that applies servo-controlled normal load via an electrically actuated ball-screw drive, which allows precise and fast control using square, triangular and sinusoidal wave functions ($\Delta\sigma_n^e$ <~0.2 MPa, response time <0.01 s). The apparatus can apply not only fast changes in σ_n^e, but also high temperatures, normal stresses and fluid pressures representative of upper-to-middle crustal conditions. For more details on the apparatus and materials, refer to Texts S1 and S2 in Supporting Information S1).

2.2. Experimental Conditions and Procedures

Previous studies have shown that the two gouge materials used exhibit closely similar frictional behavior; both show a transition from v-strengthening to v-weakening with increasing temperate (T), that is, at around 80–100°C (Chen et al., 2015; Verberne et al., 2013). In this study, the temperatures used ranged from room-T to 110°C, leading to a transition in frictional behavior from stable sliding (v-strengthening regime) to self-sustained, small-amplitude shear strength oscillations (v-neutral/weakening regime) at constant σ_n^e. The base level of normal stress ($\overline{\sigma}_n$) was set at 50, 100, 150 or 180 MPa. We applied a fixed fluid (water) pressure (p_f) of 15 MPa (vessel pressure surrounding the unjacketed sample), except in one experiment where a 3 MPa fluid pressure was used to check its effect on seal friction.

In each experiment, 0.65–0.80 g of gouge powder was distributed in the annular space between two grooved pistons and contained by an outer and inner ring (see Figure 1-inset), producing a 1.0–1.4 mm-thick gouge layer. After applying the target values of $\overline{\sigma}_n$, p_f(hence $\overline{\sigma}_n^e$), and T, we first sheared the sample at a constant load-point

10.1029/2024GL109755

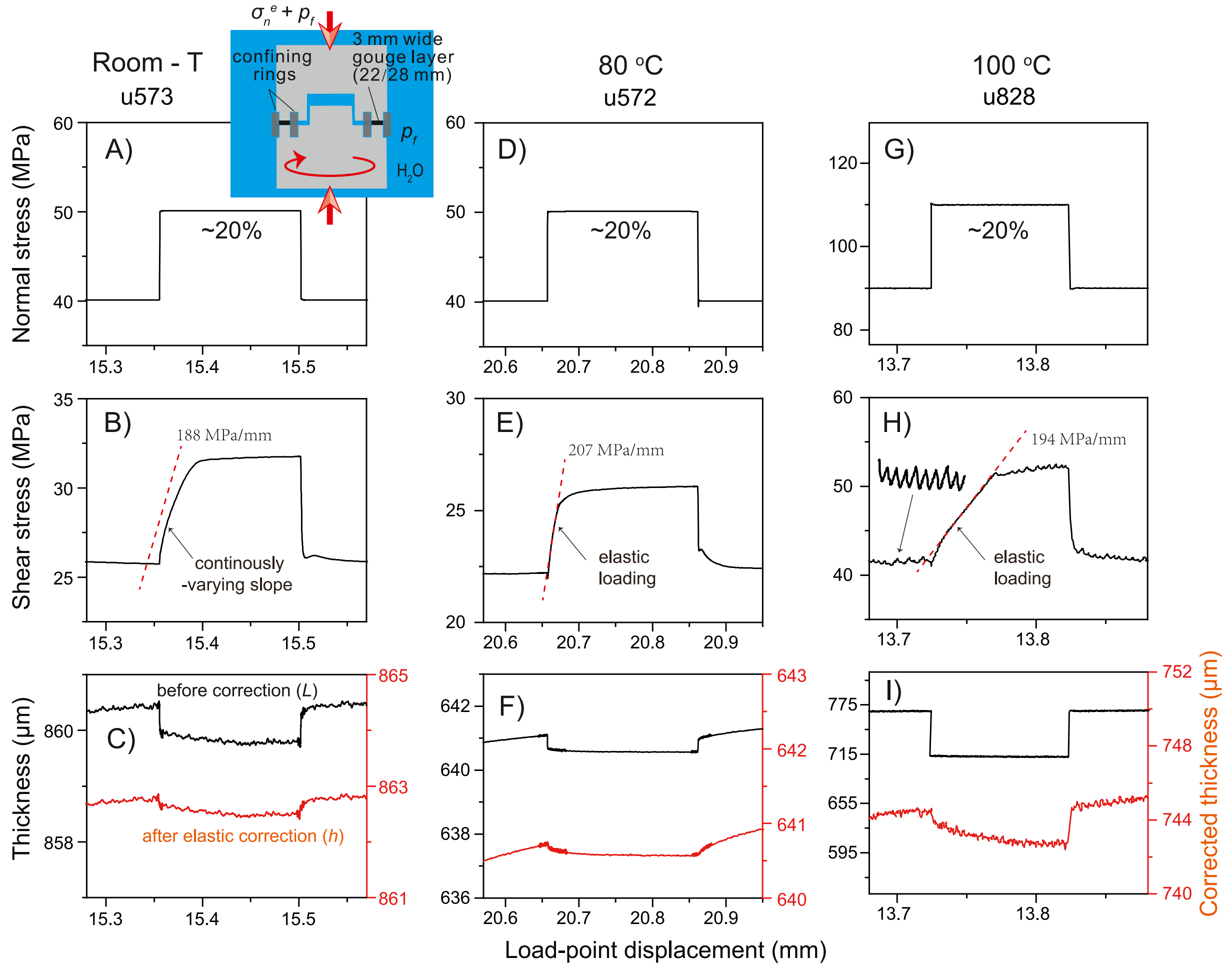

Figure 1. Results from NSS tests at room temperature (a–c), 80°C (D–F), and 100°C (g–i) hydrothermal conditions. The steps were completed within 0.2 s or 0.2 μm load-point displacement. In each test, the three panels show the evolution of normal stress, shear stress, and gouge layer thickness changes corrected for elastic deformation of sample and machine with varying normal stress, respectively. The inset shown in panel (a) illustrates the sample-piston assembly used in the present study. Note that the inner and outer superally rings prevent the gouge layer from extruding yet allow for well-drained sample conditions (i.e., easy pore fluid exchange between the sample and enclosing pressure vessel).

velocity (v_{imp}) of 1–10 μm/s through ∼7.0 mm displacement (d), subsequently stepping v_{imp} to verify the velocity dependence of friction obtained for our sample materials in previous studies. Different modes of σ_n^e-perturbations were subsequently superimposed on the base level value $\overline{\sigma}_n^e$, including normal stress steps (NSS), triangular and sinusoidal oscillations (NSO), while shearing at v_{imp} of 1 μm/s. For each perturbation mode, we systematically varied the perturbation magnitude and period (where applicable). Following Richardson and Marone (1999), in two experiments we also investigated the effects of σ_n^e-oscillations on frictional healing (NSO/H), that is, slide-hold-slide (SHS) tests were performed while oscillating σ_n^e during the hold periods. Table S1 in Supporting Information S1 summarizes the key data for all five experiments performed.

2.3. Data Processing

All quantities measured were sampled at a rate of 30–900 Hz. To calculate shear stress (τ), the externally-measured torque was corrected for dynamic seal friction using displacement- and pore pressure-dependent calibrations following Den Hartog et al. (2013). Standard error propagation analysis showed that the error in shear stress is <0.1%. The combined apparatus-sample shear stiffness (K) was determined from the shear stress versus load point displacement curve obtained during unloading of each experiment. Axial displacement (L), was measured externally using a high-resolution linear variable differential transformer (lvdt) attached to the lower forcing block (0.1 μm resolution, response time <0.01 s) and varied significantly in the present study due to varying normal stress. Note that during fast variations in applied effective normal stress σ_n^e for example, in NSO tests, L changed almost reversibly and in phase with σ_n^e. Differentiation therefore gives the "apparent" elastic stiffness of the system in the axial direction (i.e., of the apparatus and gouge layer), that is, $K_n = d\sigma_n^e/dL$ (Figure S3 in Supporting Information S1). For each experiment, we applied the K_n value obtained to correct L, thus obtaining a combined measure of anelastic plus any permanent changes in gouge thickness (h), using

$$\Delta h = \Delta L + \left(\sigma_n^e - \overline{\sigma}_n^e\right)/K_n, \tag{1}$$

where $\overline{\sigma}_n^e$ is the reference or pre-perturbation level of σ_n^e. Data on the evolution of normal stress, shear stress, and gouge layer thickness L (before correction) with shear displacement, are plotted for all the five experiments in Figure S4 in Supporting Information S1.

3. Results

3.1. Normal Stress Step (NSS) Tests

Figure 1 presents the results of all NSS tests performed at different temperatures with roughly the same step size (20%). At room temperature, the gouge showed v-strengthening, stable sliding behavior, consistent with previous work (Verberne et al., 2013). In response to a (quasi-)instantaneous upstep in effective normal stress (σ_n^e), the shear stress (τ) showed a small instantaneous increase followed by a gradual increase, at decreasing rate, to a new steady state (Figure 1b). At 80°C, the shear stress showed similar evolution, but with the early response being close to linear (Figure 1e). At 100°C, small-amplitude oscillations in shear stress (<0.5 MPa) occurred during constant-σ_n^e sliding, consistent with v-weakening. In response to an upstep, the shear stress increased nearly linearly with displacement, then abruptly transitioned toward a new mean level with superimposed small-amplitude oscillations (Figure 1h). We note that the (nearly-)linear increase in τ at 80 and 100°C follows the elastic loading path, corresponding to the combined apparatus-sample shear stiffness. At 80 and 100°C, the shear stress showed a small instantaneous decrease upon applying the σ_n^e-step, followed by a rapid increase (i.e., faster than elastic stressing rate) until reaching the linear elastic stage. Upon a downstep, the shear stress at the three temperatures showed an abrupt decrease followed by a gradual decrease to the original level. Corrected layer thickness data at all the temperatures showed transient compaction/dilation after the upstep/downstep, with an evolution distance similar to that of shear stress (Figures 1c, 1f, and 1i). At a fixed temperature, the relative response in shear stress magnitude and transient thickness change were not sensitive to step size (10%–40%, Figure S5 in Supporting Information S1).

3.2. Normal Stress Oscillation (NSO) Tests and Effects on Healing (NSO/H)

Figure 2a shows the results when a fault sliding under hydrothermal conditions is subjected to sinusoidal changes in σ_n^e, with a fixed relative amplitude ($\Delta\sigma_n^e/\overline{\sigma}_n^e = 10\%$) and varying periods ($T_{imp} = 0.1$–1,000 s). For long (>50s) and short (<2 s) periods, the τ-response was also sinusoidal and almost in phase with the σ_n^e-changes. For intermediate periods (2 s $\leq T_{imp} \leq$ 50 s), the shear stress response became irregular in shape and for some periods (5–20 s) two cyclic components appeared in one period of σ_n^e-change (Figure 2b). Interestingly, as the imposed oscillation period decreased from 20 to 0.2 s, we observed an increasing reduction in mean shear stress ($\overline{\tau}$) with respect to the preceding steady-state level (τ_{ss}), defined

$$\Delta\tau_w = \tau_{ss} - \overline{\tau}, \tag{2}$$

and hereafter referred to as "dynamic weakening." At a fixed short period (i.e., 1 s), increasing the amplitude of σ_n^e-oscillations caused increased dynamic weakening, increased oscillation amplitude in the shear stress, and an increase in corrected gouge thickness (dilation) – Figure 2c. Notably, the reduction in shear stress is reversible, that is, strength recovers when the oscillations stop (see red dashed lines and rectangle in Figures 2a and 2c). The dilation observed is unlikely to be caused by the Poisson effect of shear stress reduction, since reducing shear stress tends to cause compaction of a gouge layer (Karner & Marone, 2001, Texts S3 in Supporting Information S1).

In the NSO/H tests, shear stress showed a rapid reduction at the initiation of hold periods with simultaneously imposed NSO, followed by a gentle, on-going relaxation see first SHS-sequence in Figure 2d. Upon re-shearing,

10.1029/2024GL109755

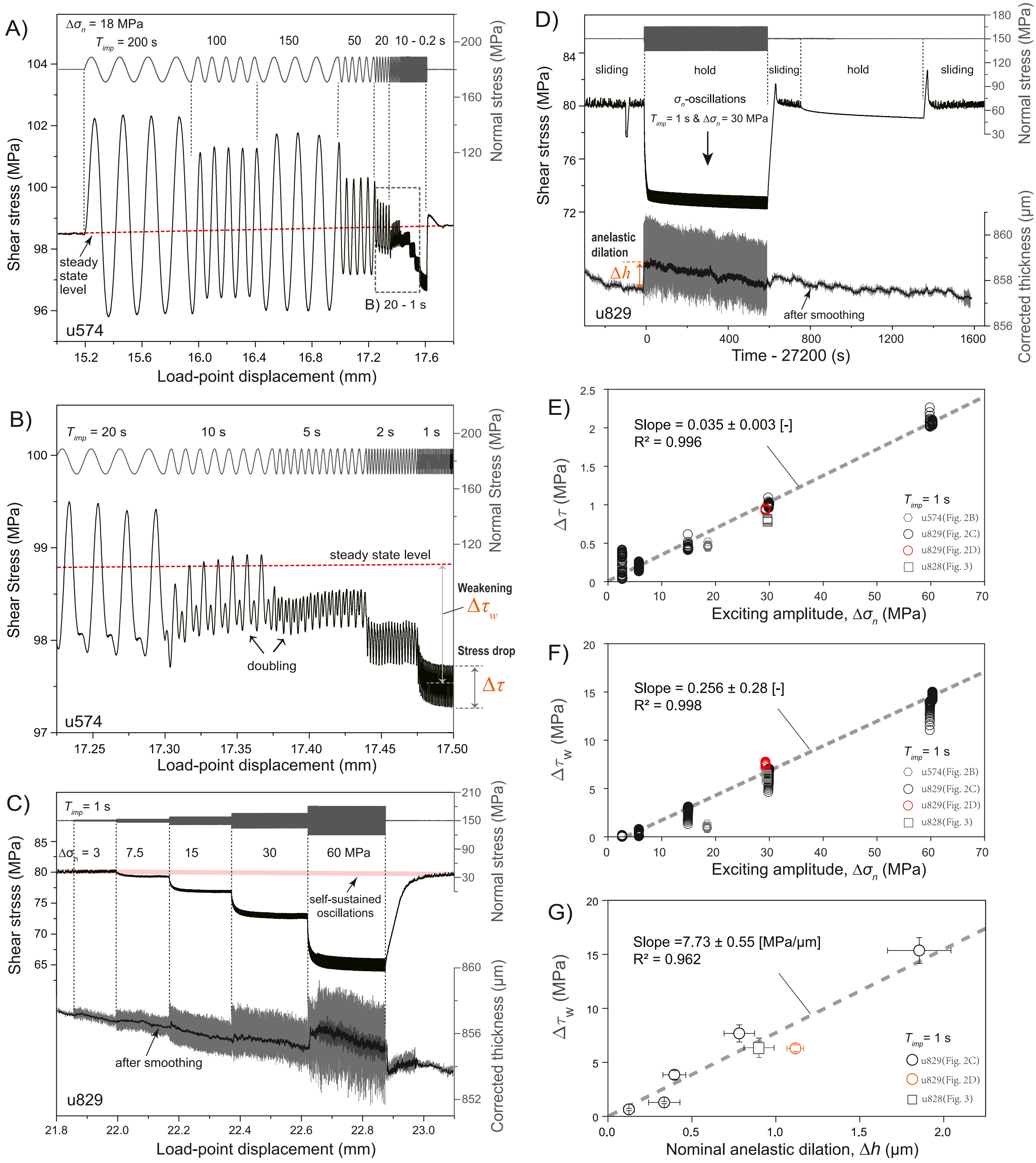

Figure 2.

the shear stress showed a rapid linear increase to a peak. The difference in peak and steady-state friction, or so-called frictional healing, is ∼1/2 that gained in a subsequent, conventional SHS-sequence, employing the same hold period (Figure 2d). Imposing fast NSO during hold periods also caused sudden dilation followed by gentle compaction, while in the conventional SHS sequence there was no dilation phase. Similar results were obtained in our second NSO/H test, which adopted the reverse perturbation sequences (σ_n^e-oscillations were imposed in the second hold period, Figure S6 in Supporting Information S1).

3.3. A Control Test

To check the robustness of the observed dilation and its correlation with dynamic weakening, we performed a control test at 100°C (u828) in which we imposed oscillating normal stress bursts ($\Delta\sigma_n = 30$ MPa, $T_{imp} = 1$ s) with different final phases (i.e., positive-vs. negative-going final half-cycles, Figure 3a). Again, imposing fast σ_n^e-oscillations caused rapid weakening accompanied by sudden dilation; and when oscillations were terminated, τ recovered gradually to the original level, via a linear initial loading phase followed by a transient, non-linear stage (Figure 3b). Interestingly, the evolution of corrected thickness (h-value) strongly depends on the final half cycle of σ_n^e-oscillations. When oscillations were terminated after a positive σ_n^e-excursion ($\sigma_n^e > \overline{\sigma}_n^e$), the compacted gouge showed dilation as sliding proceeded, closely resembling the behavior seen at the end of varying-amplitude NSO test u829, due to a final positive σ_n^e-excursion (Figure 2c). In contrast, when oscillations were terminated after a negative σ_n^e-excursion ($\sigma_n^e < \overline{\sigma}_n^e$), the gouge was in a dilated state and showed compaction upon further sliding. In both cases, the thickness evolution distances were similar to those for τ. Similar behavior was seen when using different vibration periods (Figure S7 in Supporting Information S1), but the effect was less prominent when T_{imp} was greater than 10 s, consistent with the results in Figure 2a.

Combining results from different NSO experiments, we found that the amplitude of shear stress variations ($\Delta\tau$) and dynamic weakening ($\Delta\tau_w$) at a fixed short oscillation period is linearly proportional to the $\Delta\sigma_n^e$ imposed (Figures 2e and 2f). The amplitude of dynamic weakening is also proportional to the elastically corrected dilation (Δh) observed (Figure 2g).

4. Discussion

4.1. Different Responses at Room-T Versus Hydrothermal Conditions

NSS is the most widely-used test to investigate the effects of varying σ_n^e on friction. The previous study by Linker and Dieterich (1992) recognized a three-stage response to an upstep in σ_n. This includes an "instant response" during which shear stress increases simultaneously with the σ_n-step, an "elastic response" during which shear stress evolves with load-point displacement along the system's elastic loading path, and a final "transient response" occurring over a shear displacement similar to that seen in typical v-step tests. Another type of behavior was first reported by Prakash (1998), who instead observed only a gradual τ-change. The "three-stage evolution" and "gradual change" have been observed in both fault gouges (e.g., Hong & Marone, 2005) and bare-rock surfaces (e.g., Kilgore et al., 2017). The key difference between these two behaviors is whether a linear loading stage can be distinguished. Employing new techniques to monitor fault-normal deformation, recent studies by Kilgore et al. (2012, 2017) revealed a gradual τ-response to various sizes of σ_n-steps, similar to the observation by Prakash (1998). Their fault-normal displacement (sample + machine) followed a two-stage response consisting of a large instantaneous and a smaller, gradual response with shear displacement, which is consistent with our uncorrected thickness change data (i.e., our elastic and transient changes, Figure 1). However, our NSS tests showed a gradual, nonlinear increase in shear stress at room-T, while at 100°C it increased primarily along the elastic loading path (Figure 1), with intermediate behavior occurring at 80°C where calcite is more or

Figure 2. Results from the NSO tests conducted at hydrothermal conditions. (a) Normal stress and shear stress versus load-point displacement for calcite gouge sheared at $v_{imp} = 1$ μm/s, $T = 110$°C, and $\overline{\sigma}_n$ of 180 MPa. Sinusoidal perturbations in normal stress were imposed with a fixed amplitude $\Delta\sigma_n^e = 18$ MPa and a range of vibration periods (T_{imp}) from 200 to 0.2 s. (b) Rescaling of the results at short periods (20–1 s). (c) Normal stress, shear stress, and elastically-corrected gouge layer thickness vs. displacement for calcite gouge sheared at $v_{imp} = 1$ μm/s, $T = 80$°C, and $\overline{\sigma}_n$ of 150 MPa. Sinusoidal perturbations in σ_n were imposed with a fixed T_{imp} of 1 s and varying $\Delta\sigma_n^e$ from 3 to 60 MPa. (d) Normal stress, shear stress, and corrected gouge layer thickness versus time, for two sequences of slide-hold-slide tests, both with a hold period of 600 s. In the first sequence, normal stress oscillations were imposed during the hold period (other conditions than c). Due to the hysteresis effect, the elastic changes in thickness cannot be fully corrected, so we applied a moving average smoothing with a window size of 20 data points. (e–g) Extracted data from different experiments with the same oscillation period of 1 s, showing the amplitudes of shear stress drop ($\Delta\tau$) and the weakening ($\Delta\tau_w$) as a function of imposed $\Delta\sigma_n$, as well as the relation between $\Delta\tau_w$ and the anelastic dilation (Δh). In each case, a linear fitting was conducted.

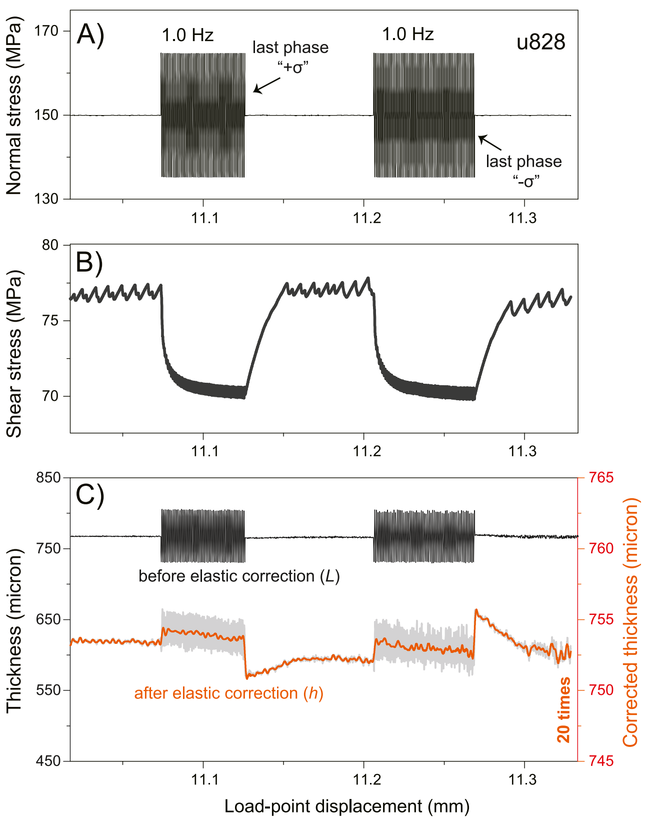

Figure 3. A pair of control NSO tests using the same vibration amplitude ($\Delta\sigma_n = 30$ MPa) and period ($T_{imp} = 1$ s), but finished with different phases ("$+\sigma$" means $\sigma_n > \bar{\sigma}_n$ in the last half period of the oscillations, while "$-\sigma$" means $\sigma_n < \bar{\sigma}_n$). (a) Normal stress, (b) shear stress, and (c) original and the corrected thickness versus time. The experiment (u828) was performed at $v_{imp} = 1$ μm/s, $p_f = 15$ MPa and $T = 100$°C.

less v-neutral (Figure S1 in Supporting Information S1). As indicated earlier, at fixed temperature, the behavior of our samples was not sensitive to imposed step size (Figure S5 in Supporting Information S1). The key question thus becomes: after a σ_n upstep, what causes the occurrence of a linear (stick) stage before sliding restarts?

Based on our observations of thickness changes, we propose that the two distinct behaviors can be explained by a dilation- and velocity-dependent friction model. It is well established that in the frictional regime shear resistance of a granular fault gouge consists of two components (ignoring cohesion), namely friction due to intergranular sliding and that due to intergranular dilation (Chen et al., 2017; Marone et al., 1990; Makedonska et al., 2011; Nakatani, 1998; Zaloj et al., 1999), which can be written as,

$$\tau \approx \tau_{gb} + \tau_{dil}. \tag{3}$$

Here, τ_{dil} expresses the shear strength required to overcome the sliding resistance offered by a compact (lower porosity) gouge under given conditions; dilation causes an increase in porosity, resulting in a more loosely compacted gouge and thus a decrease in τ_{dil} (Nakatani, 1998; Sleep, 1997). Grain boundary (gb) friction is usually described to be v-strengthening in the logarithmic form (Nakatani, 2001),

$$\mu_{gb} = \mu_{gb}{}^{*} + a ln(v_s/v^{*}). \tag{4}$$

In Equation 4, v_s is the relative v between two contacting grains, $\mu_{gb}{}^{*}$ is the gb friction at a reference velocity v^{*}, and a is the rate sensitivity. As widely recognized from laboratory experiments, an increase in v causes dilation and thus a reduction in τ_{dil} (e.g., Marone et al., 1990). The competing, opposite dependences of τ_{gb} and τ_{dil} determine the sign of the total v-dependence of shear strength of the material (Chen et al., 2017; Sleep, 1997).

Our NSS results show a gradual increase in shear stress in the v-strengthening regime ($T < 80$°C) when a fault is subjected to an upstep in σ_n^e, while in the v-weakening regime ($T > 80$°C) shear stress shows primarily linearly elastic loading (Figure 1, see also schematic in Figure S8 in Supporting Information S1). The former evolution can be simply explained by an increase in τ_{dil}, in Equation 3, caused by the observed gouge compaction. In the latter case, the competing v-dependencies of τ_{gb} and τ_{dil}, described above, play an important role. This is because, in general, for any perturbation, a v-weakening fault undergoes a larger excursion in sample slip velocity than a v-strengthening fault (Gu et al., 1984, Figure S8 in Supporting Information S1). In response to a σ_n^e-upstep, the slip rate (v_s) on a v-weakening fault (v_s) can drop instantaneously by a few orders of magnitude (e.g., Kilgore et al., 2017; Shreedharan et al., 2019). Taking the spring-slider analogue of an experimental fault, when v_s is much smaller than v_{imp}, the elastic equation for shear stress evolution $\dot{\tau} = K(v_{imp} - v_s)$ reduces to $\dot{\tau} = K v_{imp}$. We infer that the τ-evolution after a σ_n^e-upstep tends to follow the elastic-loading curve in our NSS tests at 80–100°C, because the fault becomes v-weakening (more unstable conditions) at these temperatures (Figure 1). At the same time, effects of other factors, such as slip localization and plasticity, will also change with temperature, and may play some role in affecting normal stress dependence of friction.

Finally, ee note that previous NSS experiments showing the multi-stage behavior were mostly performed on quartz-rich gouges or granitic surfaces (Hong & Marone, 2005; Linker & Dieterich, 1992). Quartz can show v-weakening at room temperature (Beeler et al., 1996; Leeman et al., 2016). Therefore, previous results on quartz gouges are not in conflict with our results or interpretations.

4.2. Dynamic Weakening and Dilation Associated With Fast Oscillations

Our study shows marked frictional weakening of a shearing fault gouge (i.e., $\Delta\tau_w/\Delta\sigma_n^e \leq 0.256$) when subjected to fast σ_n^e-oscillations (i.e., T_{imp}<10 s, Figure 2f). A similar but smaller reduction in friction was also observed in NSO tests on powdered quartz gouges at room-T/humidity conditions ($\Delta\tau_w/\Delta\sigma_n^e \leq 0.1$) by Boettcher and Marone (2004). This type of weakening effect is also of interest in other fields, especially in mechanical engineering, where imposing vibrations in the normal direction has been used to manipulate the friction of interfaces filled with lubricants (Skåre & Ståhl, 1992). However, the vibration frequencies used to induce weakening in these other fields are much higher than used here (120–6,000 Hz, Bureau et al., 2000; Drummond, 2012; Heuberger et al., 1998; Vidal et al., 2019). Friction experiments performed on dry glass bead layers has also shown that vibrating the sharing layer by passing seismic waves (center frequency ∼40 kHz) can cause dynamic weakening followed by shear stress recovery, resembling our observations (Johnson et al., 2012). As previously noted present friction theories (and mechanisms) cannot satisfactorily account for such weakening behavior (Boettcher & Marone, 2004; Bureau et al., 2000; Heuberger et al., 1998; Lastakowski et al., 2015; Vidal et al., 2019). Based on the following three arguments, we propose that the weakening might be linked to the anelastic dilation we observed.

First, systematic thickness changes in our control experiment provide a robust observation of dilation caused by fast σ_n^e-oscillations (Figure 3). A similar amount of dilation was observed at different fluid pressures but otherwise similar conditions (3 vs. 15 MPa, Figure 2g), which rules out the possibility that weakening is due to hysteresis in apparatus seal friction or to fluid pressurization of the gouge layer (different fluid pressures result in varying seal friction and pore water compressibility). Pore fluid pressurization is further excluded as the weakening mechanism because it cannot account for the dilation observed after oscillations cease (Figure 3).

Second, the NSO/H (normal stress oscillation/hold) tests showed that imposing fast σ_n^e-oscillations during a hold period resulted in faster and larger shear stress relaxation than a conventional hold sequence (Figure 2d), which is consistent with previous experiments under nominally dry conditions (Richardson & Marone, 1999). However, the magnitude of frictional healing that we obtained under vibrating σ_n^e is less than in our conventional SHS test, which is opposite to the finding by Richardson and Marone (1999). Moreover, our NSO/H tests showed a small net dilation, due to immediate dilation followed by gradual compaction over the hold period (Figure 2d), while Richardson and Marone reported larger continuous compaction (∼7× larger strain) during the same hold duration. This all suggests that the shear stress evolution is strongly tied to the compaction/dilation state of the gouge layer (Figure S8 in Supporting Information S1).

Third, the dilation- and velocity-dependent friction model (Equation 3) used in explaining our step tests can be applied to our oscillation tests. Specifically, in the NSO tests, dynamic weakening upon imposing oscillations, and the recovery of shear stress after terminating oscillations, can be attributed to the instant dilation and the subsequent transient compaction observed, through Equation 3. Whether a sticking (elastic loading) stage emerges after oscillation will be determined by the excursion of v_s (Equation 4). Following the same rationale, in the NSO/H tests, oscillations reduce compaction during hold and thus lead to reduced healing upon reshear (Figure S8 in Supporting Information S1). Qualitatively, the weakening and anelastic thickness change seen in both NSO and NSO/H tests are roughly linearly related (Figure 2g), agreeing with insights from existing friction-dilation models (Chen & Spiers, 2016; Sleep, 1997).

The above analyses demonstrate the internal consistency of the thickness and shear stress responses between different modes of perturbations. Recent gouge friction experiments without σ_n^e-perturbations have documented highly time-resolved dilation accompanying fast and slow stress-drop procedures (Hu et al., 2023). One remaining question is which process causes the dilation accompanying NSO in our tests. As discussed above, oscillation-induced fluidization or pressurization is unlikely to be the mechanism. Up to now, oscillation-induced dilation has not been documented in macroscopic gouge-type friction experiments. Boettcher and Marone (2004) did report minor dilation induced by normal stress oscillations, but it was believed to be a transient response as the fault weakened. However, both dilation and accelerated slip have been induced by fast vibrations in microscale experiments on glass beads and quartz sands, using the shear force apparatus at nominally dry conditions (Heuberger et al., 1998; Nasuno et al., 1998). In the physics literature, dilation (increase in effective thickness or reduction in coordination contact number) of the frictional layer, along with dynamic weakening, have also been reported for sliding nanoscale contacts in computer simulations–using atomistic molecular dynamics as well as discrete element and other modeling approaches (Capozza et al., 2009; Ferdowsi et al., 2015; Gao et al., 1998; Thompson & Grest, 1991; Zaloj et al., 1999). A future study will seek a physics-based explanation for, and conduct numerical simulations of, the anelastic dilation and weakening that we have observed, taking into account previous work by, for example, Bureau et al., 2000; Chen & Spiers, 2016; Perfettini et al., 2001; Sleep, 1997.

4.3. Implications for Triggered and Induced Seismicity

Our results show that fast σ_n^e-variations can cause marked fault weakening, which may be highly relevant to the triggering of earthquakes or avalanches by stress changes induced by seismic waves. The associated dilatant effect may be of great importance not only for understanding the weakening process but also in providing a key observable that might be used in monitoring.

We have shown that the weakening effect depends on both vibration amplitude and period: it occurs only at periods below a critical value. Our results thus support the notion that the dynamics are controlled by the (maximum) rate of change of normal stress ($d\sigma_n/dt$, *cf.* Lastakowski et al., 2015; Wang et al., 2020). More experiments are required to confirm this. The present experiments give a critical period of ~10s for a carbonate fault. This value is expected to vary with fault conditions, such as driving velocity (Boettcher & Marone, 2004; Bureau et al., 2000). Simply applying a linear scaling and a background driving rate of 10^{-9} m/s (~30 mm/year), the critical period increases to 5.5 hr. In future, it will be important to establish any critical oscillation period that may induce weakening of, and seismic slip on, faults in geo-energy/storage reservoirs, to guide safe injection/production operations.

5. Conclusions

We explored the effects of rapidly varying effective normal stress (σ_n^e) on fault strength by conducting rotary-shear friction experiments on simulated carbonate fault gouges under well-drained hydrothermal conditions, maintaining fluid pressure nearly constant. Upon imposing step changes in σ_n^e, the gouge thickness showed an instantaneous response followed by a transient evolution. The shear stress responses for different temperatures and perturbation sizes showed that there is no strict boundary between the three- and single stage behaviors observed by Linker and Dieterich (1992) and Prakash (1998), but that the response depends on v-dependence of friction. The occurrence of an elastic loading (stick) stage is favored by more unstable (v-weakening friction) conditions, that is, >80°C in our tests. We also observed marked weakening and dilation upon imposing fast σ_n^e-oscillations. The larger the amplitude, the larger the dilation and weakening. We proposed a theoretical argument that qualitatively captures both the present and previous observations, including the behavior seen in σ_n^e-step tests and the dynamic weakening during fast oscillations. Our results highlight that when σ_n^e is affected by human activities in the subsurface, caution should be exercised regarding the amplitude and period of the changes or cycles imposed.

Data Availability Statement

Experimental raw data are all freely available online at Chen and Niemeijer (2022).

Acknowledgments
This study is co-supported by the National Science Foundation (4217040794) and the DeepNL project (Science4Steer).

References

Beeler, N. M., & Lockner, D. A. (2003). Why earthquakes correlate weakly with the solid Earth tides: Effects of periodic stress on the rate and probability of earthquake occurrence. *Journal of Geophysical Research*, *108*(B8), 2391. https://doi.org/10.1029/2001jb001518

Beeler, N. M., Tullis, T. E., Blanpied, M. L., & Weeks, J. D. (1996). Frictional behavior of large displacement experimental faults. *Journal of Geophysical Research*, *101*(B4), 8697–8715. https://doi.org/10.1029/96jb00411

Boettcher, M. S., & Marone, C. (2004). Effects of normal stress variation on the strength and stability of creeping faults. *Journal of Geophysical Research*, *109*(B3), B03406. https://doi.org/10.1029/2003jb002824

Bureau, L., Baumberger, T., & Caroli, C. (2000). Shear response of a frictional interface to a normal load modulation. *Physics Reviews E*, *62*(5), 6810–6820. https://doi.org/10.1103/physreve.62.6810

Capozza, R., Vanossi, A., Vezzani, A., & Zapperi, S. (2009). Suppression of friction by mechanical vibrations. *Physical Review Letters*, *103*(8), 085502. https://doi.org/10.1103/physrevlett.103.085502

Cappa, F., Scuderi, M. M., Collettini, C., Guglielmi, Y., & Avouac, J.-P. (2019). Stabilization of fault slip by fluid injection in the laboratory and in situ. *Science Advances*, *5*(3), eaau4065. https://doi.org/10.1126/sciadv.aau4065

Chambon, G., & Rudnicki, J. W. (2001). Effects of normal stress variations on frictional stability of a fluid-infiltrated fault. *Journal of Geophysical Research*, *106*(B6), 11353–11372. https://doi.org/10.1029/2001jb900002

Chen, J., & Niemeijer, A. R. (2022). Data accompanying the paper entitled "Rapid normal stress oscillations cause dilatation and weakening in gouge-bearing faults". (Version 2) [Dataset]. *4TU.ResearchData*. https://doi.org/10.4121/19500344.v2

Chen, J., Niemeijer, A. R., & Spiers, C. J. (2017). Microphysically derived expressions for rate-and-state friction parameters, a, b, and Dc. *Journal of Geophysical Research*, *122*(12), 9627–9657. https://doi.org/10.1002/2017jb014226

Chen, J., & Spiers, C. J. (2016). Rate and state frictional and healing behavior of carbonate fault gouge explained using microphysical model. *Journal of Geophysical Research*, *121*(12), 8642–8665. https://doi.org/10.1002/2016jb013470

Chen, J., Verberne, B. A., & Spiers, C. J. (2015). Interseismic re-strengthening and stabilization of carbonate faults by "non-Dieterich" healing under hydrothermal conditions. *Earth and Planetary Science Letters*, *423*, 1–12. https://doi.org/10.1016/j.epsl.2015.03.044

Cochard, A., Bureau, L., & Baumberger, T. (2003). Stabilization of frictional sliding by normal load modulation. *Journal of Applied Mechanics*, *70*(2), 220–226. https://doi.org/10.1115/1.1546241

Dang, W., & Konietzky, H. (2022). The effect of normal load oscillation amplitude on the frictional behavior of a rough basalt fracture. *Rock Mechanics and Rock Engineering*, *55*(6), 3385–3397. https://doi.org/10.1007/s00603-022-02815-w

Den Hartog, S. A. M., Niemeijer, A. R., & Spiers, C. J. (2013). Friction on subduction megathrust faults: Beyond the illite-muscovite transition. *Earth and Planetary Science Letters*, *373*, 8–19. https://doi.org/10.1016/j.epsl.2013.04.036

Drummond, C. (2012). Electric-field-induced friction reduction and control. *Physical Review Letters*, *109*(15), 154302. https://doi.org/10.1103/physrevlett.109.154302

Ellsworth, W. L. (2013). Injection-induced earthquakes. *Science*, *341*(6142), 1225942. https://doi.org/10.1126/science.1225942

Ferdowsi, B., Griffa, M., Guyer, R. A., Johnson, P. A., Marone, C., & Carmeliet, J. (2015). Acoustically induced slip in sheared granular layers: Application to dynamic earthquake triggering. *Geophysical Research Letters*, *42*(22), 9750–9757. https://doi.org/10.1002/2015gl066096

French, M. E., Zhu, W., & Banker, J. (2016). Fault slip controlled by stress path and fluid pressurization rate. *Geophysical Research Letters*, *43*(9), 4330–4339. https://doi.org/10.1002/2016gl068893

Gao, J., Luedtke, W. D., & Landman, U. (1998). Friction control in thin-film lubrication. *Journal of Physical Chemistry B*, *102*(26), 5033–5037. https://doi.org/10.1021/jp982150q

Griffa, M., Ferdowsi, B., Guyer, R. A., Daub, E. G., Johnson, P. A., Marone, C., & Carmeliet, J. (2013). Influence of vibration amplitude on dynamic triggering of slip in sheared granular layers. *Physics Reviews E*, *87*(1), 012205. https://doi.org/10.1103/physreve.87.012205

Gu, J. C., Rice, J. R., Ruina, A. L., & Tse, S. T. (1984). Slip motion and stability of a single degree of freedom elastic system with rate and state dependent friction. *Journal of the Mechanics and Physics of Solids*, *32*(3), 167–196. https://doi.org/10.1016/0022-5096(84)90007-3

Heuberger, M., Drummond, C., & Israelachvili, J. (1998). Coupling of normal and transverse motions during frictional sliding. *The Journal of Physical Chemistry B*, *102*(26), 5038–5041. https://doi.org/10.1021/jp9823143

Hill, D. P., Reasenberg, P. A., Michael, A., Arabaz, W. J., Beroza, G., Brumbaugh, D., et al. (1993). Seismicity remotely triggered by the Magnitude 7.3 Landers, California, earthquake. *Science*, *260*(5114), 1617–1623. https://doi.org/10.1126/science.260.5114.1617

Hong, T., & Marone, C. (2005). Effects of normal stress perturbations on the frictional properties of simulated faults. *Geochemistry, Geophysics, Geosystems*, *6*(3), Q03012. https://doi.org/10.1029/2004gc000821

Hu, W., Ge, Y., Xu, Q., Huang, R., Zhao, Q., Gou, H., et al. (2023). High time-resolved studies of stick–slip show similar dilatancy to fast and slow earthquakes. *Proceedings of the National Academy of Sciences*, *120.47*(47), e2305134120. https://doi.org/10.1073/pnas.2305134120

Johnson, P. A., Carpenter, B., Knuth, M., Kaproth, B. M., Le Bas, P.-Y., Daub, E. G., & Marone, C. (2012). Nonlinear dynamical triggering of slow slip on simulated earthquake faults with implications to Earth. *Journal of Geophysical Research*, *117*(B4), B04310. https://doi.org/10.1029/2011jb008594

Karner, S. L., & Marone, C. (2001). Frictional restrengthening in simulated fault gouge: Effect of shear load perturbations. *Journal of Geophysical Research*, *106*(19), 319–337.

Kilgore, B., Beeler, N. M., Lozos, J., & Oglesby, D. (2017). Rock friction under variable normal stress. *Journal of Geophysical Research*, *122*(9), 7042–7075. https://doi.org/10.1002/2017JB014049

Kilgore, B., Lozos, J., Beeler, N., & Oglesby, D. (2012). Laboratory observations of fault strength in response to changes in normal stress. *Journal of Applied Mechanics*, *79*(3). https://doi.org/10.1115/1.4005883

Lastakowski, H., G'eminard, J. C., & Vidal, V. (2015). Granular friction: Triggering large events with small vibrations. *Scientific Reports*, *5*(1), 13455. https://doi.org/10.1038/srep13455.gd

Leeman, J. R., Saffer, D. M., Scuderi, M. M., & Marone, C. (2016). Laboratory observations of slow earthquakes and the spectrum of tectonic fault slip modes. *Nature Communications*, *7*(1), 11104. https://doi.org/10.1038/ncomms11104

Linker, M. F., & Dieterich, J. H. (1992). Effects of variable normal stress on rock friction: Observations and constitutive equations. *Journal of Geophysical Research*, *97*(B4), 4923–4940. https://doi.org/10.1029/92jb00017

Lockner, D. A., & Beeler, N. M. (1999). Premonitory slip and tidal triggering of earthquakes. *Journal of Geophysical Research*, *104*(B9), 20133–20151. https://doi.org/10.1029/1999jb900205

Makedonska, N., Sparks, D. W., Aharonov, E., & Goren, L. (2011). Friction versus dilatation revisited: Insights from theoretical and numerical models. *Journal of Geophysical Research*, *116*(B9), B09302. https://doi.org/10.1029/2010JB008139

Marone, C., Raleigh, C. B., & Scholz, C. H. (1990). Frictional behavior and constitutive modeling of simulated fault gouge. *Journal of Geophysical Research*, *95*(B5), 7007–7025. https://doi.org/10.1029/JB095iB05p07007

Nakatani, M. (1998). A new mechanism of slip-weakening and strength recovery of friction associated with the mechanical consolidation of gouge. *Journal of Geophysical Research*, *103*(B11), 27239–27256. https://doi.org/10.1029/98JB02639

Nakatani, M. (2001). Conceptual and physical clarification of rate and state friction: Frictional sliding as a thermally activated rheology. *Journal of Geophysical Research*, *106*(B7), 13347–13380. https://doi.org/10.1029/2000jb900453

Nasuno, S., Kudrolli, A. B. A., & Gollub, J. P. (1998). Time-resolved studies of stick-slip friction in sheared granular layers. *Physical Review E - Statistical Physics, Plasmas, Fluids, and Related Interdisciplinary Topics*, *58*(2), 2161–2171. https://doi.org/10.1103/physreve.58.2161

Niemeijer, A. R., Spiers, C. J., & Peach, C. J. (2008). Frictional behaviour of simulated quartz fault gouges under hydrothermal conditions: Results from ultra-high strain rotary shear experiments. *Tectonophysics*, *460*(1–4), 288–303. https://doi.org/10.1016/j.tecto.2008.09.003

Noël, C., Pimienta, L., & Violay, M. (2019). Time-dependent deformations of sandstone during pore fluid pressure oscillations: Implications for natural and induced seismicity. *Journal of Geophysical Research*, *124*(1), 801–821. https://doi.org/10.1029/2018jb016546

Olsson, W. A. (1988). The effects of normal stress history on rock friction, key questions in rock mechanics. In P. A. Cundall, R. L. Sterling, & A. M. Starfield (Eds.), *Proceedings of the 29th U.S. Symposium* (pp. 111–117). University of Minnesota, Balkema.

Passelègue, F. X., Brantut, N., & Mitchell, T. M. (2018). Fault reactivation by fluid injection: Controls from stress state and injection rate. *Geophysical Research Letters*, *45*(23), 12837–12846. https://doi.org/10.1029/2018gl080470

Perfettini, H., Schmittbuhl, J., Rice, J. R., & Cocco, M. (2001). Frictional response induced by time-dependent fluctuations of the normal loading. *Journal of Geophysical Research*, *106*(B7), 13455–13472. https://doi.org/10.1029/2000jb900366

Prakash, V. (1998). Frictional response of sliding interfaces subjected to time varying normal pressures. *Journal of Tribology*, *120*(1), 97–102. https://doi.org/10.1115/1.2834197

Richardson, E., & Marone, C. (1999). Effects of normal stress vibrations on frictional healing. *Journal of Geophysical Research*, *104*(B12), 28859–28878. https://doi.org/10.1029/1999jb900320

Scuderi, M. M., & Collettini, C. (2016). The role of fluid pressure in induced vs. triggered seismicity: Insights from rock deformation experiments on carbonates. *Scientific Reports*, *6*(1), 24852. https://doi.org/10.1038/srep24852

Scuderi, M. M., Collettini, C., & Marone, C. (2017). Frictional stability and earthquake triggering during fluid pressure stimulation of an experimental fault. *Earth and Planetary Science Letters*, *477*, 84–96. https://doi.org/10.1016/j.epsl.2017.08.009

Segall, P., & Rice, J. R. (1995). Dilatancy, compaction, and slip instability of a fluid-infiltrated fault. *Journal of Geophysical Research*, *100*(B11), 22155–22171. https://doi.org/10.1029/95jb02403

Shreedharan, S., Rivière, J., Bhattacharya, P., & Marone, C. (2019). Frictional state evolution during normal stress perturbations probed with ultrasonic waves. *Journal of Geophysical Research*, *124*(6), 5469–5491. https://doi.org/10.1029/2018jb016885

Skåre, T., & Ståhl, J.-E. (1992). Static and dynamic friction processes under the influence of external vibrations. *Wear*, *154*(1), 177–192. https://doi.org/10.1016/0043-1648(92)90253-5

Sleep, N. H. (1997). Application of a unified rate and state friction theory to the mechanics of fault zones with strain localization. *Journal of Geophysical Research*, *102*(B2), 2875–2895. https://doi.org/10.1029/96jb03410

Thompson, P. A., & Grest, G. S. (1991). Granular flow: Friction and the dilatancy transition. *Physical Review Letters*, *67*(13), 1751–1754. https://doi.org/10.1103/physrevlett.67.1751

Verberne, B. A., Spiers, C. J., Niemeijer, A. R., De Bresser, J. H. P., DeWinter, D. A. M., & Plümper, O. (2013). Frictional properties and microstructure of calcite-rich fault gouges sheared at sub-seismic sliding velocities. *Pure and Applied Geophysics*, *171*(10), 2617–2640. https://doi.org/10.1007/s00024-013-0760-0

Vidal, V., Oliver, C., Lastakowski, H., Varas, G., & Géminard, J.-C. (2019). Friction weakening by mechanical vibrations: A velocity-controlled process. *The European Physical Journal E*, *42*(7), 91. https://doi.org/10.1140/epje/i2019-11855-2

Wang, L., Kwiatek, G., Rybacki, E., Bonnelye, A., Bohnhoff, M., & Dresen, G. (2020). Laboratory study on fluid-induced fault slip behavior: The role of fluid pressurization rate. *Geophysical Research Letters*, *47*(6), e2019GL086627. https://doi.org/10.1029/2019GL086627

Xing, T., Zhu, W., French, M., & Belzer, B. (2019). Stabilizing effect of high pore fluid pressure on slip behaviors of gouge-bearing faults. *Journal of Geophysical Research*, *124*(9), 9526–9545. https://doi.org/10.1029/2019jb018002

Zaloj, V., Urbakh, M., & Klafter, J. (1999). Modifying friction by manipulating normal response to lateral motion. *Physical Review Letters*, *82*(24), 4823–4826. https://doi.org/10.1103/physrevlett.82.4823